catalysts

MDPI

Review

Surface Passivation Engineering for Photoelectrochemical Water Splitting

Jingying Shi [1,2,3,*], Xuefei Zhao [2,3] and Can Li [2,3]

[1] Center of Materials Science and Optoelectronics Engineering, University of Chinese Academy of Sciences, Beijing 100049, China
[2] State Key Laboratory of Catalysis, Dalian Institute of Chemical Physics, Chinese Academy of Sciences, Dalian National Laboratory for Clean Energy, Zhongshan Road 457, Dalian 116023, China
[3] University of Chinese Academy of Sciences, Beijing 100049, China
* Correspondence: jingyingshi@dicp.ac.cn

Abstract: Surface passivation engineering is an imperative way to improve photoelectrode performance for photoelectrochemical (PEC) water splitting. To the best of our knowledge, it has never been systematically reviewed in a feature article. In this review, we summarize various passivation materials and their preparation, characterizations by PEC measurements and some related spectral technologies. We highlight the features of the passivation effect that separate it from other modifications, such as cocatalyst decoration, and we demonstrate significant progress in combining surface passivation engineering with other interfacial modification strategies for the rational design of photoelectrodes. Ideas for future research on surface passivation modification for improving the performance of photoelectrodes are also proposed.

Keywords: surface passivation; photoelectrochemical; water splitting; modification

check for updates

Citation: Shi, J.; Zhao, X.; Li, C. Surface Passivation Engineering for Photoelectrochemical Water Splitting. *Catalysts* **2023**, *13*, 217. https://doi.org/10.3390/catal13020217

Academic Editors: Eun Duck Park, Won Bae Kim and Ji-Wook Jang

Received: 29 December 2022
Revised: 12 January 2023
Accepted: 12 January 2023
Published: 17 January 2023

Copyright: © 2023 by the authors. Licensee MDPI, Basel, Switzerland. This article is an open access article distributed under the terms and conditions of the Creative Commons Attribution (CC BY) license (https://creativecommons.org/licenses/by/4.0/).

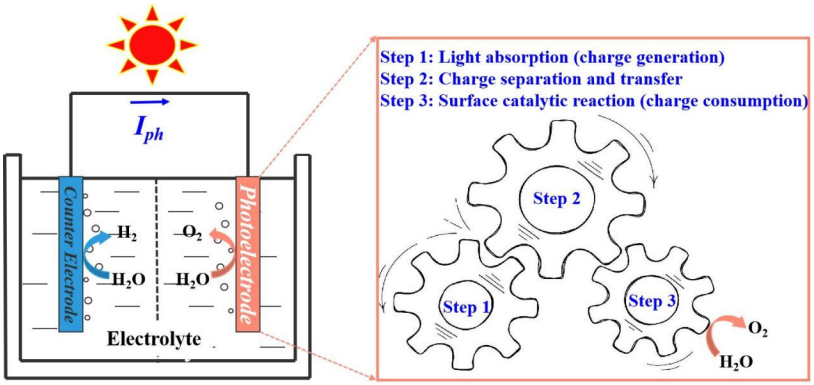
1. Introduction

Since the commencement of the 21st century, human society has entered a rapid development period thanks to the fast advancements of high technologies. Then along came an unprecedented increase in energy consumption for human beings. At present, global energy consumption is almost 20 TW per year [1,2]. Fossil fuels, including coal, oil and natural gas, have long been the primary energy sources since the Industrial Revolution, which started almost three hundred years ago in Europe. In addition to the anxiety about the irreversible depletion of fossil resources, in recent years, humans have been confronted with more and more challenges from the greenhouse effect, extreme weather, environmental pollution and a deteriorated ecological system due to huge carbon emissions from the utilization of carbon fossil energy.

As a huge energy reservoir, the sun delivers carbon-free and renewable energy up to 10,000 TW to the Earth's surface per year, which is quite sufficient to meet the energy requirements of human beings [2,3]. Therefore, developing solar utilization is very desirable in order to realize carbon neutrality and energy sustainability. Apart from natural photosynthesis by plants, human beings have explored various strategies to harvest, convert and/or store solar energy for use in electricity, chemicals (such as hydrogen) and heat, which can be used routinely in human society. Among these, photoelectrochemical (PEC, also referred to as photoelectrocatalytic) water splitting provides a very promising way to cost-effectively produce clean hydrogen via solar water splitting, which was pioneered by Fujishima and Honda in 1972 [4].

The PEC reaction is performed in a PEC cell that should at least comprise a photoelectrode, counter electrode and electrolyte, very similar to the structure of traditional electrochemical cells (Scheme 1 with photoanode is an example). Photoelectrodes are generally photocatalyst particulars/films deposited on a conductive substrate or semiconducting

crystal, such as TiO_2, with ohmic contact in some cases (more details are available in our previous book chapter [1]). Once illuminated, the photoelectrode is excited to generate charge carriers, which then move to the solid/solution interface for participation in the chemical reaction. As such, charge carriers in photoelectrodes suffer a three-step process, including generation, separation and transfer, and final consumption by a PEC half-reaction (Scheme 1).



Scheme 1. PEC cell and PEC process for solar water splitting (with photoanode as an example).

The efficiencies for these three steps together determine the half-cell efficiency for the PEC process, which can be described as the following equation [5,6]:

$$\eta_{\mathrm{half-cell}} = \eta_{\mathrm{abs}} \times \eta_{\mathrm{sep-trans}} \times \eta_{\mathrm{cat}} \quad (1)$$

$\eta_{\mathrm{half-cell}}$ represents the solar conversion efficiency for the half-reaction in the PEC cell, η_{abs} is the light absorption efficiency, which decides the producing amount of charge carriers, $\eta_{\mathrm{sep-trans}}$ represents charge separation and transfer efficiency (against energy loss due to charge recombination), determining the fraction of surviving charge carriers, which can reach the interfacial active sites, and η_{cat} represents the interfacial catalytic efficiency, indicating those portions of the charge carriers able to overcome the barrier for irreversible reaction. Among these three steps and efficiencies, light absorption is relatively independent, while the other two steps are often coupled with each other. There are already some comprehensive review articles addressing photocatalyst materials (nitrides, oxynitrides, sulfides, etc.) with wide visible light absorption [7–9]. In addition, light absorbers with special morphologies, such as a nanorod, nanotube, nanoflower or elaborate surface antireflection layer, are very helpful for boosting light harvesting or improving the collecting of the minority carriers [10]. However, up until the present, those photoelectrodes with a single component light absorber have never achieved satisfying energy conversion efficiency despite a band edge absorption beyond 600 nm. An efficient photoelectrode is always multicomponent and integrated, which may be ascribed to the multi-step process of PEC reactions themselves, and the η_{cat} can often be remarkably improved by integrating the light absorber with the surface electrocatalyst, therefore, resulting in the enhanced $\eta_{\mathrm{half-cell}}$. Several reviews and perspectives have addressed this topic, including our previous review article concerning transition-metal-based electrocatalysts as cocatalysts for photoelectrochemical water splitting [11–15]. There were also some reports demonstrating that the cocatalysts were able to indirectly facilitate the charge carriers' transfer and separation in addition to providing active reaction sites [16]. Regardless, for a photoelectrode with the same light absorber and cocatalyst, we could evaluate and compare the charge separation and transfer ability, thus developing corresponding strategies to improve the $\eta_{\mathrm{half-cell}}$. To a great extent, studying how to boost $\eta_{\mathrm{sep-trans}}$ (step 2 in Scheme 1) is very crucial, beyond all doubt, to tap into the potential of light absorption materials to achieve a high $\eta_{-\mathrm{cell}}$ approaching theoretical values.

Defect states are commonly present in the material bulk and surface, and they are inclined to trap carriers and act as charge recombination centers, which results in energy loss during the charge transfer process. Bulk defects generally can be eliminated by improving crystallinity or doping, while surface defects need to be removed by passivation. Therefore, surface passivation has been extensively accepted to be a pivotal interfacial engineering strategy to obtain highly efficient photoelectrodes, which is frequently mentioned or discussed in some review articles [17–20]. However, to the best of our knowledge, it has never been systematically reviewed in a feature article.

In this review, we summarize various passivation overlayers and their preparation, characterizations by PEC measurements and some related spectral technologies. The role of passivation that separates the cocatalyst and heterojunction is highlighted. We also demonstrate recent significant progress in combining surface passivation engineering with other interfacial modification strategies for the rational design of photoelectrodes. Suggestions for future research on surface passivation modification for improving the performance of photoelectrodes are proposed.

2. Surface Passivation Engineering for Photoelectrodes

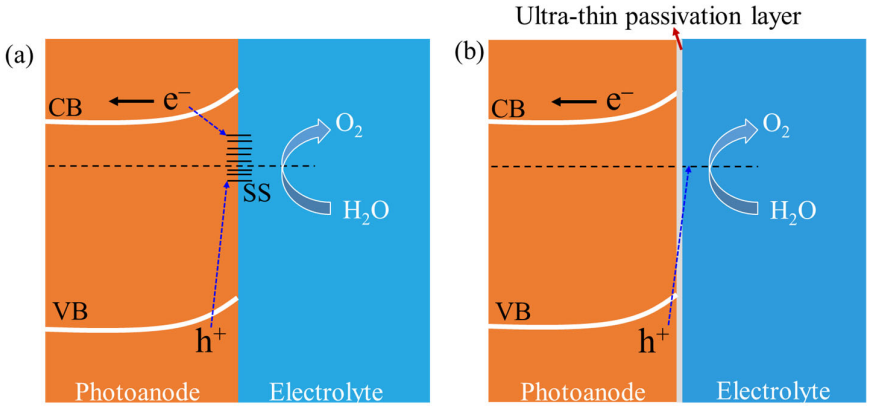
2.1. Background and Fundamentals

The passivation strategy was adopted early in the PV industry to deal with dangling bonds in bulk amorphous silicon, as well as surface defects in single-crystal silicon due to interrupted surface lattice [14,18]. This method has been extended to dye-sensitized solar cells, invented by Gratzel et al., in which some insulator or semiconducting thin films, such as Al_2O_3, Ga_2O_3, MgO or ZrO_2, were coated on a porous TiO_2 substrate to increase the open circuit potential thanks to their significant reduction in electron recombination [21]. Then, in recent decades, it was further extended to modify photoelectrodes for improved PEC water splitting in view of a similar working principle and requirement in suppressing charge recombination between them.

Generally, in most cases, the semiconducting light absorbers on photoelectrodes are nanocrystalline materials with ultrahigh, true surface areas in order to boost light absorption, as well as offer more active sites for absorption and reaction. However, such materials have a double-edged sword effect with rich surface states (or surface defect states), which may act as carrier trapping centers and induce surface Fermi level pinning so as to restrict surface band bending [22–25] in thermodynamics, and dynamically, the photogenerated charges would firstly inject into the surface traps before they can transfer from the solid to the solution and participate chemical reactions, resulting in the production of additional overpotential other than a reaction kinetics barrier (Scheme 2). This point has been regarded as an important factor for the significant retardation of the photocurrent onset potential in comparison with the flat-band potential of the semiconductor light absorber, which causes an unreasonably low photovoltage [23,26]. With this in mind, efforts have been dedicated to eliminating surface traps through passivation engineering.

Hematite (α-Fe_2O_3) is a prototypical photoanode material for a surface passivation study due to its intrinsically abundant surface defect state originating from short-range structural disorders near the surface [20,27]. Bisquert and Hamann et al. used electrochemical impedance spectroscopy (EIS) to identify the roles of the surface state for a water oxidation reaction over a hematite photoanode [28]. They prepared a series of thin film hematite photoanodes by atomic layer deposition (ALD) and measured the IS during a PEC water oxidation process as a function of applied bias potential, incident light intensity and solution pH. After analysis by fitting via an equivalent circuit, it was found that when the surface trap capacitance was located at the peak position (i.e., maximum), the charge transfer resistance of holes to the donor species was almost right in the valley (i.e., minimum) under the same experimental conditions. This result suggests that photogenerated holes trapped and accumulated in the surface states rather than those directly from the valence band participate in the water oxidation reaction. In other words, the water oxidation reaction would not occur until a sufficient number of holes were collected by the surface

states. This work reveals the surface state plays a crucial role in the hole-transfer step on the defect-rich photoelectrode surface. In this regard, the presence of the surface state is detrimental to the PEC performance, which clearly induces an energy loss mechanism.



Scheme 2. Photoanode/electrolyte interface for PEC water oxidation reaction (**a**) in the presence of surface states (SS) and (**b**) in the presence of passivation layer to remove the surface states.

2.2. Surface Self-Passivation

Aiming at eliminating redundant surface states, Wang et al. proposed the re-growth strategy (100 °C growth for 1 h, then 800 °C annealing for 5 min) to reconstruct the hematite surface [27]. It is seen from the morphology evolution observation (Figure 1a–h) that the original random surface structure (sdH sample) was improved to be orderly after the second re-growth post-treatment (rgH II sample), while the overgrowth sample (rgH III) demonstrated random surface again. The current-potential curves shown in Figure 1i indicate a negative shift beyond 380 mV in onset potential for the re-growth samples in comparison with those of the ALD-grown sample (denoted as aH). With the further decoration of NiFeOx cocatalyst, the turn-on voltage of the hematite shifts more negatively and generates a photovoltage high as 800 mV.

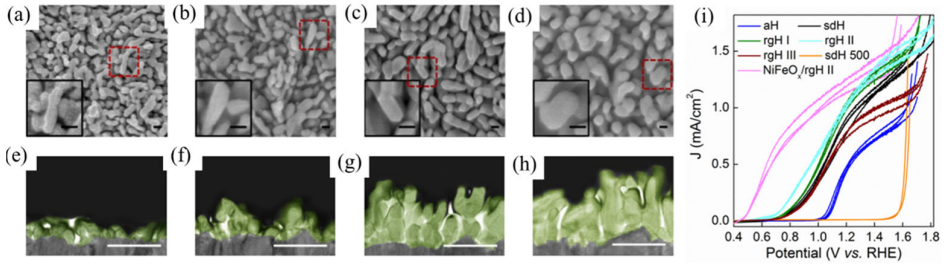


Figure 1. Morphology evolution of hematite as a result of the re-growth treatments. Scanning electron micrographs image of (**a**) sdH, (**b**) rgH I, (**c**) rgH II and (**d**) rgH III; scale bars, 100 nm. Magnified views of selected areas in the main frames are presented in the insets. Transmission electron micrographs of focused ion beam prepared cross-sectional samples of (**e**) sdH, (**f**) rgH I, (**g**) rgH II and (**h**) rgH III, scale bars, 500 nm. (**i**) Comparison of PEC performances of aH, sdH, rgH I, rgH II, rgH III and NiFeOx/rgH II samples. The photocurrents of sdH 500 (annealed at 500 °C) were less than 10 μA. Reproduced from [27] with permission.

Fathabadi et al. employed electrochemical cyclic voltammetry to in situ grow a passivation layer over Ti-doped Fe_2O_3 photoanode, and the optimized bias potential was 0–1.2 V vs. Ag/AgCl [29]. This overcoating was identified to be an ultra-thin amorphous Ti/K co-doped defective α-Fe_2O_3-x, which led to about 60% enhancement in the PEC activity regardless of constant photocurrent onset potential. Additionally, this passivation layer made the photocurrent retention up to 99% and 95% after 10 and 96 hours of PEC tests, respectively. The long-term stability was ascribed to the successive in situ passivation

during a PEC cycling test and the decreased leaching rate of Fe and Ti ions due to the physical isolation from the electrolyte.

Light exposure treatment has been reported to be another method to optimize PEC activity due to the suppression of surface energy losses [30–32]. Berlinguette et al. demonstrated the formation of a surface passivation layer over $BiVO_4$ photoanode after suffering ultraviolet (UV) irradiation for an extended time period of 20 h [30]. Electrochemical measurements indicated that the charge carrier density was over ten-fold higher, together with a cathodic shift of 250 mV after photolysis treatments. XPS analysis suggested a diminishing number of surface defect states (possible dangling oxygen sites) for the photolyzed photoanodes. Consequently, such UV exposure treatment produces a cathodic shift of about 230 mV in onset potential and makes the photocurrent double at 1.23 V vs. reversible hydrogen electrode (RHE, same below without otherwise stated), which is nearly comparable to the effect of surface cocatalyst modification.

2.3. Inorganic Passivation Layers

In most cases, surface passivation engineering was put into effect with ultra-thin insulating or wide bandgap oxides, such as Al_2O_3, Ga_2O_3, TiO_2, SiO_2, ZrO_2, MoO_3 and some (oxy)sulfides, metal, etc. [26,33–37]. Sivula et al. investigated the effect of an Al_2O_3 overlayer deposited by the ALD method on the PEC performance of hematite photoelectrode [26]. The self-limited preparation method allowed for the conformal film on nanostructured hematite with an atomic level of 0.15–2 nm in thickness. PEC measurement results indicated a negative shift of 100 mV for the onset potential and increased the photocurrent by a factor of 3.5 (from 0.24 mA cm^{-2} to 0.85 mA cm^{-2} at 1.0 V in 1 M NaOH solution). The light-off cathodic transient peak was observed from the transient current–time curves at low biases of 0.9 and 1.1 V (Figure 2a), which could be assigned to electrons diffusing from the external circuit to recombine with the accumulated holes at the semiconductor–liquid junction (SCLJ). The peak area represents the accumulated charges at the SCLJ, which are estimated to be 71.2 μC cm^{-2} and 198 μC cm^{-2} at 1.1 V, respectively. This result indicates a decreasing hole accumulation at the SCLJ after passivation treatment. The EIS analysis suggested that the interfacial charge transfer for water oxidation begins when the capacitance drops abruptly, highly in accordance with the above-mentioned characteristic role for surface states. In addition, the induced photoluminescence (PL) for the Al_2O_3-modified hematite photoanode implied that a portion of the inter-bandgap surface states had been passivated (Figure 2b).

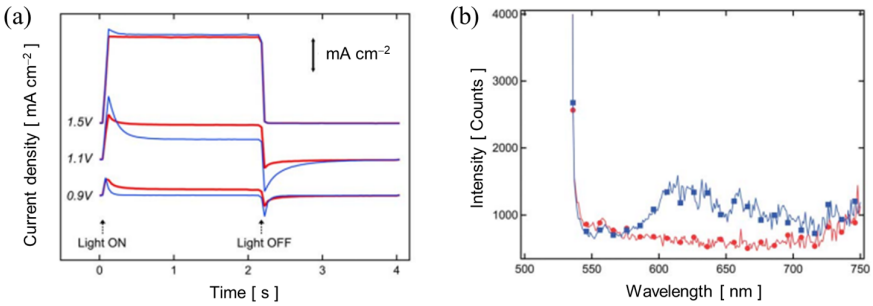


Figure 2. (**a**) Transient photoresponse shown by light chopping current densities (light on/light off) as a function of time. The bias potentials were applied for 4 s (2 s with light on and 2 s with light off) at 0.9, 1.1 and 1.5 V, as indicated. Comparison of the transient behavior of iron oxide photoanodes with 3 ALD cycles of Al_2O_3 overlayer (red, thick line) and without (blue, thin line). (**b**) Photoluminescence emission spectra (excitation wavelength = 520 nm) of a hematite cauliflower-type nanostructure photoanode before (red circles) and after 3 ALD cycles of Al_2O_3 on its surface (blue squares). Reproduced from [26] with permission.

Subsequently, the same group compared Al_2O_3, Ga_2O_3 and In_2O_3 as passivation layers for a hematite thin film (27–30 nm thick) photoanode fabricated by spray pyrol-

ysis [33]. The overlayers were deposited by a chemical bath based on urea hydrolysis, such as the above ALD Al_2O_3 overlayer. They demonstrated the passivating effect by negatively shifting the onset potential and increasing the photocurrent density as well. Among them, Ga_2O_3 achieves the best results. A larger negative shift of up to 200 mV in onset potential was achieved on a Ga_2O_3-coated film. Under the protection of the Ga_2O_3 passivation layer, the photoanode was able to keep sustainable water splitting in an alkaline solution for 30 h. Recently, the In_2O_3 thin layer with a thickness of a few nanometers was coated over a titanium-doped hematite photoanode [38]. The turn-on potential was almost constant before and after modification. However, the photocurrent density was largely improved from 1.2 mA cm^{-2} to 3.4 mA cm^{-2}. The authors ascribed the high PEC activity to surface passivation in addition to the heterojunction formed between hematite and In_2O_3 overcoating.

Other than decoration on hematite photoanode, noncatalytic alumina layer had been extensively applied on $BiVO_4$ [34], WO_3 [39], Ta_3N_5 [40,41], TiO_2 nanotube arrays [42], TiO_2 nanorods [43,44], $ZnFe_2O_4$ [45] and InGaN/Si double-junction photocathodes [46] as a surface passivation layer to facilitate charge transfer for PEC reaction. All of these passivation modifications show a smaller effect with a cathodic shift of no more than 100 mV in V_{on} and less than a 10% increase in J_{ph}. Occasionally, a negative effect was reported. For example, the ALD Al_2O_3 overlayer decorated on $BiVO_4$ photoanodes had been found to be very detrimental to the PEC activity with a significant decrease in J_{ph} regardless of its thickness (ALD 1, 10 and 100 cycles) [34]. This adverse effect was ascribed to the poor conductivity of Al_2O_3 films by the authors. Then the authors removed the Al_2O_3 overlayer by soaking it in 1 M NaOH aqueous solution with stirring for 0.5 h, and the obtained sample was denoted as p-$BiVO_4$. Unexpectedly, the three p-$BiVO_4$ samples all delivered higher J_{ph} than the $BiVO_4$ with and without Al_2O_3 overlayers. The optimal J_{ph} is up to 1.34 mA/cm^2, which is 73% higher than that of the naked $BiVO_4$. The authors proposed that the surface oxygen defects were passivated during the deposition and subsequent removal of the Al_2O_3 overlayer, which accounted for the enhanced PEC performance of the $BiVO_4$ photoanode.

Passivation layer thickness is an important factor that often needs to be optimized for improving PEC performance. Choi et al. compared the effect of alumina overlayer by ALD 3 cycles (~0.5 nm), 30 cycles (~5 nm) and 300 cycles (~50 nm) on the PEC activity of WO_3 photoanode [39]. The photocurrent density displayed a bit, three-fold increase and complete loss, respectively (Figure 3a). The thick overlayer may cause a surface reaction site blockage or high resistance to prevent charge transfer so as to lose the activity. On the other hand, it is seen that the onset potential stays constant despite the presence of the passivation layer in all cases. In view of this point, the authors thought that the Fermi pinning was yet fixed in spite of alumina deposition. Moreover, the authors compared the oxygen evolution Faradaic efficiencies and photocurrent in a test duration of 2 h. The Faradaic efficiency for Al_2O_3/WO_3 was three times that of WO_3 (54.1% vs. 17.7%), while the passing electrical quantity for the former was much less than three times of the latter. It was thus proposed that the increased photocurrent resulted not only from the alumina passivation but also from the inhibition of peroxo-species formation to a great degree (Figure 3b). The further characterization of the time-resolved absorption spectroscopy (TAS) indicated that the passivation decreased the electron trapping while it increased the population of trapped holes on WO_3, thus generating a positive effect on PEC performance.

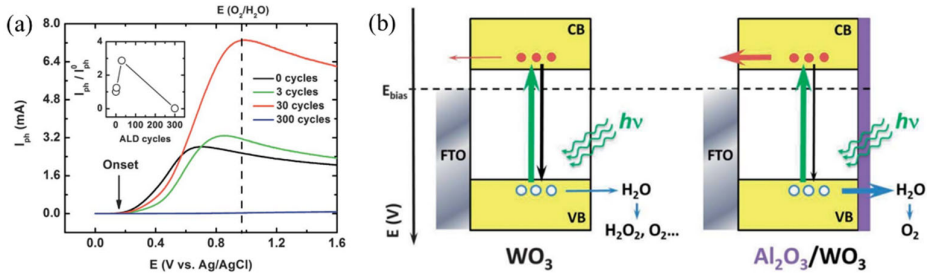


Figure 3. (**a**) Voltammetric response of transparent Al_2O_3/WO_3 electrodes under simulated AM 1.5 G illumination (120 mW cm^{-2}). The alumina overlayer was deposited by ALD for 0 cycles (black), 3 cycles (green), 30 cycles (red) and 300 cycles (blue). Electrolyte: Ar-purged 0.1 M $HClO_4$ (pH 1.0). Scan rate: 20 mV s^{-1}. The photocurrent (I_{ph}) was obtained by correcting the capacitive contribution in the dark. Inset: normalized photocurrent values taken at 0.97 V (vs. Ag/AgCl) (thermodynamic potential of water oxidation at pH 1.0) as a function of ALD cycles. (**b**) Schematic illustration of hole- and electron-mediated charge transfer occurring on WO_3 (left) and Al_2O_3/WO_3 (right) illuminated electrodes biased at a potential around the thermodynamic water oxidation potential (0.97 V vs. Ag/AgCl). The purple rectangle on the right side represents the alumina overlayer. For the sake of clarity, electrons (red, full circles) and holes (blue, open circles) are represented as free on the conduction (CB) and valence (VB) bands, respectively. Likewise, blue and red arrows represent hole and electron-mediated processes, respectively. Green arrows represent the photogeneration of electron–hole pairs. Black arrows represent recombination losses. Relative arrow thicknesses represent the rate of the processes (the thicker the arrow, the faster and more effective the process). Reproduced from [39] with permission.

Silicon is also a typical light absorption material, which inherently has rich surface defects that needs to be treated. Since silicon itself is rather active in reacting with the surrounding trace amounts of oxygen gas, a silicon oxide overcoating is almost inevitably accompanied by a fresh silicon surface to be a natural passivation layer [14]. On account of large charge-transport resistance, the SiO_x coating generally should be controlled within several nm of thickness [47–49]. Sometimes an additional passivation layer, such as a TiO_2 thin-film layer, is required to combine with a self-oxidized SiO_2 for better passivation and physical protection against electrolyte corrosion [47]. TiO_2 and Ta_2O_5 thin films are able to act as passivation layers for silicon nanowires [50] and amorphous silicon [51], as well as InAs/p-Si composite photoelectrodes [52]. Several sulfides, such as CoS_2 and $MoOS_x$ modification, also have been reported to enable the p-type silicon microwire arrays to be passivated, meanwhile, they play the role of cocatalyst [53,54].

Liu et al. reported a $(NiFeCoCe)O_x$ multicomponent overlayer to modify $BiVO_4$ photoanode in which the roles of each metal oxide were discussed and identified principally by comparing the PEC behavior with and without a sacrificial agent of H_2O_2 [55]. It was concluded that poor catalytic CeO_x shows a passivation-only effect, FeO_x shows a bifunction of moderate passivation and catalysis, and NiO_x and CoO_x show a catalysis-only effect. In addition, $(NiFe)O_x$ acts as the surface catalytic component and $(CoFeCe)O_x$ as the charge capture/collection component. Therefore, the roles of surface engineering films are actually complicated and ambiguous. In general, noncatalytic materials, such as Al_2O_3, Ga_2O_3, In_2O_3, CeO_x, SiO_2 and TiO_2, would be less disputed for functioning as a passivation layer. The passivation effect of the catalytic materials, such as CoO_x, CoPi, CoS_2 and $MoOS_x$, is a controversial problem since the cocatalyst function often dominates the modification effect.

To address the above dispute point, Wang et al. investigated the surface engineering effect of a well-known cocatalyst thin film of $NiFeO_x$ (~10 nm thick) over hematite photoanodes by three different preparation methods [56]. They principally used intensity-modulated photocurrent spectroscopy (IMPS) technology to determine the surface charge transfer rate constant (k_{tran}) and surface charge recombination rate constant (k_{rec}), which reflected the effectivity of hole transfer from the semiconductor to the solution and surface

charge recombination due to the presence of surface states, respectively. The decoration of the surface $NiFeO_x$ for all photoanodes did not induce an enhanced k_{tran} as expected in the case of water oxidation cocatalyst modification. In contrast, the values for k_{tran} were equal to or smaller than those naked samples. In Figure 4a, it is seen that the re-growth (rgH) photoanode with a $NiFeO_x$ overlayer shows a slower k_{tran} and a much slower k_{rec} than the other two samples. In Figure 4b, the GaO_x-coated hematite displays similar results in comparison with that without GaO_x modification. This result may suggest that $NiFeO_x$ has the same passivation effect as GaO_x. In Figure 4c, the authors listed and compared the k_{tran} and k_{rec} for ALD hematite (aH) with and without deposition of $NiFeO_x$ thin film at a bias potential of 1.1 V. Clearly, the $NiFeO_x$ decoration doesn't alter the k_{tran} but largely decreases the k_{rec}. Therefore, it confirmed the passivation role of the $NiFeO_x$ overcoating. From this work, the authors argued that the traditional cocatalyst of $NiFeO_x$ thin film primarily serves as a passivation layer rather than a catalytic layer over hematite-based photoanodes. IMPS offers a quantitative measurement of the surface charge transfer kinetics, which is helpful for identifying the effect of surface modification.

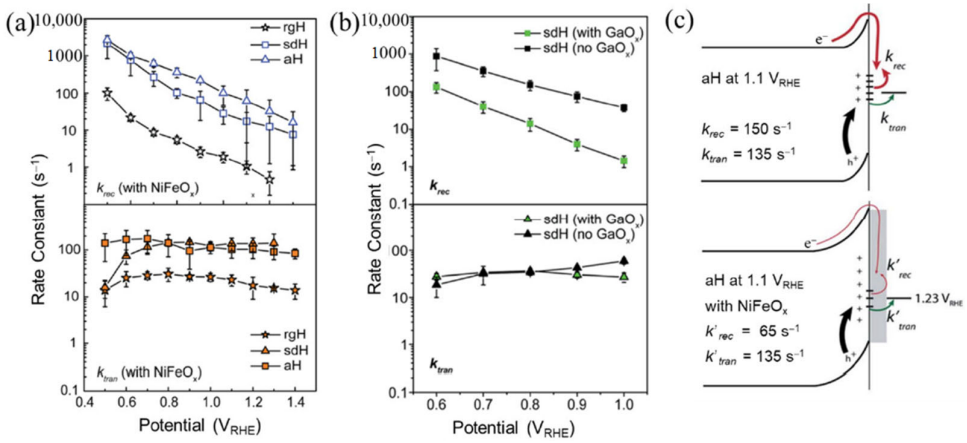


Figure 4. (**a**) Rate constants for hematite photoelectrodes with $NiFeO_x$ surface decorations. Top: recombination rate constants for photoelectrodes by three different preparation methods; bottom: surface charge transfer rate constants for the same photoelectrodes. The error bars are standard deviations between different samples. (**b**) Rate constants for hematite treated with GaO_x passivation. Top: recombination; bottom: transfer. (**c**) Surface decorations on hematite improve the overall PEC performance by reducing surface recombination. Compared with bare hematite (top), $NiFeO_x$ does not change k_{tran} (bottom). Instead, it reduces the recombination rate constant (k_{rec}) greatly. Reproduced from [56] with permission.

Some metals, such as nickel, have been reported as a physical passivation layer for perovskite photoanode, which generates about a six-fold enhanced photocurrent [57]. However, taking account of the easy self-development of NiO_x or NiOOH (known catalysts) on the top surface of metallic nickel during the PEC water oxidation reaction [58,59], it is hard to attribute the barely improved PEC activity to the passivation effect. The role of surface metal is difficult to define since it almost integrates with other properties, such as catalysis, charge transfer, junction, physical isolation, etc.

2.4. Metal-Organic Framework-Based Passivation Layers

Metal-organic frameworks (MOFs) comprising metal clusters and organic ligands are a class of porous materials that have great advantages in surface functionalization [60,61]. With this in mind, some MOFs have tentatively been applied to photoelectrodes for surface engineering [62–66].

Zeolitic imidazolate framework-8 (ZIF-8) was first applied as a surface passivation layer over ZnO photoanodes to boost PEC water splitting [62,63]. It was fabricated via the solvothermal method with the underlying ZnO nanorods as self-sacrificial templates

and thus built a core-shell structure, as shown in Figure 5a,b [62]. The surface defect states were just removed during the growth of the ZIF-8 overlayer derived from the surface dissolution of the ZnO nanorods under solvothermal conditions. Accordingly, the ZIF-8 film is conformal with tunable thickness, which is usually required to generate a passivation effect. The decoration of the 3–5 nm thick ZIF-8 overcoating leads to a remarkable enhancement in photocurrent density and a negative shift in onset potential for a water oxidation reaction (current–potential curves are shown in Figure 5d). ZIF-8 is optically transparent in the UV–visible range, which does not block the incident light. Moreover, the chemically inert and conformal coating helps ZnO photoanode achieve an excellent PEC stability of 3 h in an alkaline solution of 0.1 M KOH. Integrating with $Ni(OH)_2$ nanosheet cocatalyst results in further increasing PEC activity (Figure 5c,d). On the other hand, the authors employed time-resolved PL and Raman spectroscopy together with electron paramagnetic resonance (EPR) to offer evidence for the passivation effects of ZIF-8 thin film.

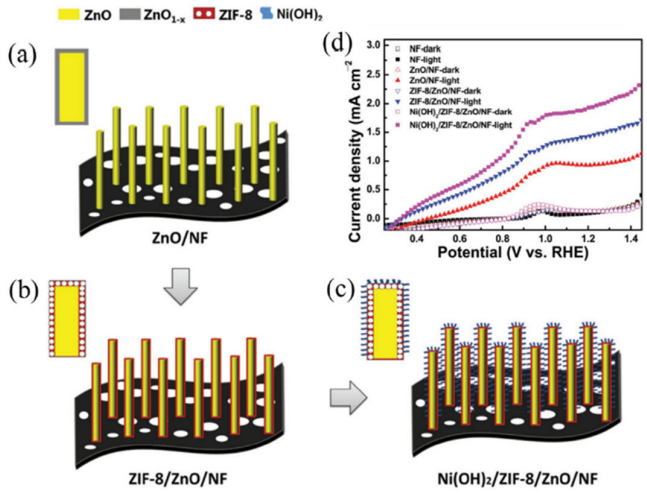


Figure 5. (**a**–**c**) Schematic illustration of the fabrication processes of $Ni(OH)_2$/ZIF-8/ZnO/NF photoanode. The inset depicts the variation of surface chemistry. (**d**) LSV curves for typical photoanodes ($Ni(OH)_2$/ZIF-8/ZnO/NF, ZIF-8/ZnO/NF, ZnO/NF, NF) in the dark and under AM 1.5 G irradiation in 0.1 M KOH electrolyte. Reproduced from [62] with permission.

Ultrathin Fe MOF, Co MOF and FeCo biMOF have been used to passivate the surface defects of hematite, and all of them showed a positive effect on enhancing PEC activity [64–66]. However, in addition to passivation, all of them are recognized as cocatalysts for PEC water oxidation, and FeCo biMOF plays a role of heterojunction as well [66]. Therefore, the MOF often demonstrates multi-functional properties apart from the passivation effect. The MOF-modified photoelectrodes are still quite few, which needs more investigation.

2.5. Organic Passivation Layers

In contrast with inorganic materials, very limited organic compounds have been reported to be effective passivation layers for photoelectrodes, which may be due to photodegradation, hydrophobic and their poor conductivity nature. Organic sulfides, such as thioacetamide and octadecylthiol, were explored early to passivate the III-V semiconductors of InAs and InP, respectively, in dry environments [67,68]. Recently, surface modification with some organic materials was demonstrated to enable boosting of the PEC performances for GaN and Si photoelectrodes [25,69,70].

The organic sulfide 1,2-ethanedithiol (EDT) may be the first one that acts as an effective surface passivation layer to significantly improve the PEC performance of GaN nanowires (NWs) photocathodes [25]. It is seen in Figure 5a,b that the photocurrent density sharply increases from 1.85 mA/cm^2 to 31 mA/cm^2 at 0.2 V; meanwhile, the turn-on voltage shifts from −0.35 to 0.1 V after EDT modification. The passivation effect results from the

decreasing number of chemisorbed -OH and -O bonds on the GaN surface via XPS analysis. The room-temperature PL spectra indicate a 24-times stronger band-edge emission intensity for the EDT-NWs than that for the untreated NWs (Figure 6c). The band edge recovery was ascribed to the eliminating nonradiative recombination centers by force of passivation. Another experimental evidence is proposed from the time-resolved photoluminescence (TRPL) results. The fast and slow decay time constants (τ1 and τ2), calculated from a double exponential decay fitting, are listed in Figure 6d. EDT-NWs display a slower decay (τ2) than the untreated-NWs, indicating an EDT passivation effect due to the removal of surface states. PEC stability is sharply prolonged from 4 h to 55 h upon EDT decoration. Apart from passivation, the other possible roles of the EDT, such as cocatalyst or heterojunction, were not discussed.

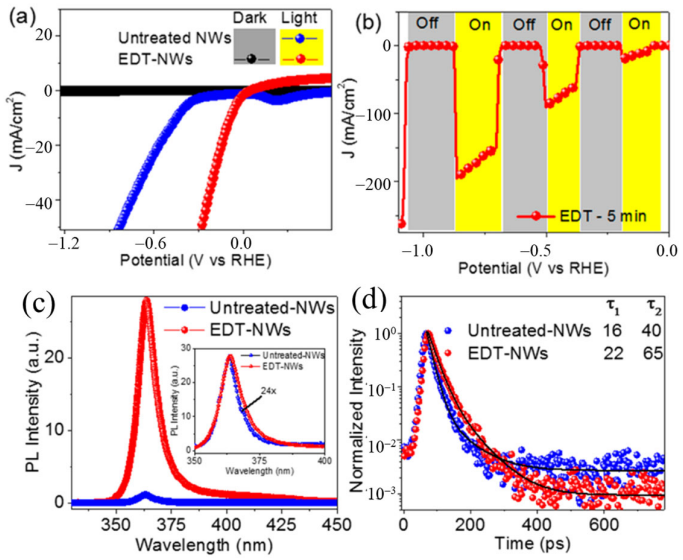


Figure 6. (**a**) Linear sweep voltammetry of untreated NWs and EDT-NWs. (**b**) Chopped illumination J−V curve of EDT-NWs. (**c**) Room-temperature PL of untreated NWs and EDT-NWs. The inset in (**c**) shows the untreated NWs' intensity multiplied by 24 to normalize it with the PL intensity of the EDT-NWs. (**d**) TRPL carrier lifetimes of the untreated-NWs and EDT-NWs. The fast and slow decay time constants (τ1 and τ2) are indicated in the figure. Reproduced from [25] with permission.

A well-known hole charge layer material of poly(3,4-ethylene dioxythiophene): polystyrene sulfonate (PEDOT:PSS) in organic photovoltaic cells has been used as surface decoration on n-type silicon photoanode in PEC conversion of I^- into I_3^- ions, which generated a record-high photovoltage of 657 mV among Si-based photoanodes [69]. With a microwave photoconductance decay (μ-PCD) technique, the minority carrier lifetimes for the textured silicon before and after PEDOT:PSS decoration were estimated to be 23.8 μs and 37.7 μs. The remarkably extended carrier lifetime directly evidences the passivated silicon. On the other hand, PEDOT:PSS is considered to play another role in constructing heterojunctions with silicon light absorbers.

In view of the above examples, surface passivation with organic overlayers can be a very efficient way to improve the PEC performance (as summarized in Table 1). Moreover, unlike time-consuming, energy-intensive preparations for the inorganic passivation layer, the solution methods for the deposition of organic thin films are generally simple, facile and precise, which makes organic modification very promising for highly efficient solar-to-chemical conversion.

Table 1. Optimized PEC performances of the representative photoelectrodes with surface passivation.

Photoelectrode	Passivation Layer	Onset Potential Shift (mV)	Photocurrent Density (mA cm^{-2})		Reference
			Before Passivating	After Passivating	
α-Fe_2O_3	FeO_x	−380	0.6	1.2	[27]
α-Fe_2O_3	Al_2O_3	−100	# 0.24	# 0.85	[26]
WO_3	Al_2O_3	0	0.6	1.8	[39]
ZnO	ZIF-8	−100	0.92	1.45	[62]
GaN	EDT	+450	* 1.85	* 31	[25]

At bias potential of 1.0 V; * at bias potential of 0.2 V; others at bias potential of 1.23 V.

3. Rational Designs of Efficient Photoelectrodes Based on Passivation Layer

3.1. Superiorities and Limitations of Surface-Passivation-Only Modification

As indicated above, surface passivation engineering has been developed to be an effective method for boosting the PEC performance of photoelectrodes. However, it is not always effective in improving PEC performance. For example, Sivula et al. found that ultra-thin TiO_2 overlayer modification moves neither the photocurrent density nor the onset potential, suggesting no influence on the Fe_2O_3 photoanode [26]. Even negatively, the Al_2O_3 overlayers prepared via 1–100 cycles ALD all result in decreased PEC activity of the $BiVO_4$ photoanodes [34].

On the other hand, the effects on the PEC performance of photoelectrodes due to surface-passivation-only treatment are actually limited, which shifts the onset potential within 200 mV and makes it hard to generate photocurrent density with fold increases in most of the reported cases. Moreover, although onset potential shift is a representative effect yielded by passivation, it sometimes remains almost unchanged with bare enhancement in the photocurrent. The significantly improved PEC performances are frequently achieved when the passivation overlayer plays other roles, such as cocatalyst or heterojunctions [53,54,64–66,69]. Actually, in view of the complicated multi-step processes for the PEC process, it is unsubstantial to rely on single-function materials to obtain efficient photoelectrodes. As such, combing a passivation overlayer with a cocatalyst and/or other functional materials, such as a charge or transfer layer, to fabricate integrated photoelectrodes appears to be a well-accepted method for highly efficient and durable PEC conversion. Herein, some typical examples are briefly shown for the rational design of efficient photoelectrodes based on a passivation layer.

3.2. Integration of Surface Passivation and Cocatalyst

Integrating the passivation layer and cocatalyst is a favored and efficient way for high-performance photoelectrodes through an accelerated interfacial transfer of charge carriers preserved by surface passivation engineering. Like other ferrites, the $ZnFe_2O_4$ photoanode shows poor PEC activity for water oxidation reaction due to its inherently low charge mobility and abundant surface defects as charge recombination centers [2]. To address this issue, Jae Sung Lee et al. introduced a thin TiO_2 passivation interlayer between the underlying $ZnFe_2O_4$ dendrite/SnO_2 helix and overlying $NiFeO_x$ cocatalyst [71]. The presence of the TiO_2 passivation layer gave rise to a cathodic shift of about 100 mV in onset potential and a two-fold increase in photocurrent at 1.23 V, and the integrated photoanode yielded a record-high photocurrent density of about 1 mA cm^{-2} at 1.23 V among the previous $ZnFe_2O_4$ based photoanodes.

Ji-Hyun Jang et al. found that the nanoporous hematite photoanode with a Ti-doped SiO_x passivation overlayer delivered a photocurrent density of 2.44 mA cm^{-2} at 1.23 V. Once it was further decorated with a cobalt phosphate cocatalyst, a high photocurrent density reaching 3.19 mA cm^{-2} at 1.23 V with excellent PEC stability could be achieved [72].

In this respect, jointly using a passivation layer and cocatalyst modification shows great superiority over their sole application.

3.3. Integration of Surface Passivation and Hole-Storage Layer

Tandem nitride is a very attractive candidate for photoanode material due to its wide visible light absorption and suitable energy band levels [73–79]. Unfortunately, it shares the common inherent drawback of nitrides—a heavy reconstruction overcoating (~2 nm thick), which is composed of the incomplete nitrides and oxides of TaN and TaO, as indicated in Figure 7a [75]. To deal with these surface defects, Li et al. implemented a passivation treatment by cooling the as-prepared tandem nitrides under a mixture of Ar and O_2 (O_2/Ar = 0.2%), and the resulting sample was denoted as Ta_3N_5(P). This post-treatment passivates the surface states and constructs a shorter range of structural disorders (Figure 7b). The PEC measurements revealed a cathodic shift onset potential of 130 mV and three-fold increased photocurrent at 1.23 V after the passivation treatment (Figure 7c). Then the Ta_3N_5(P) suffers step-by-step layer modification with an amorphous TiO_x, Ni(OH)x/Ferrihydrite and IrCo-complex molecular, which act as blocking layer, hole-storage layer and cocatalyst, respectively. The resulting complex 2/complex 1/$Ni(OH)_x$/Fh/TiO_x/Ta_3N_5(P) photoanode demonstrated a high fill factor and a photocurrent density of 12.1 mA/cm^2 at 1.23 V, approaching the theoretical limit of 12.9 mA/cm^2 for tandem nitride under sunlight (Figure 7d). Although the hole-storage layer is a very effective modification strategy for photoanodes [73–78] and photocathodes [80], the passivation treatment helps to preserve the photogenerated charges from loss in surface defect recombination and thus results in efficient extraction by the hole-storage layer for surface reaction. Namely, combing the surface passivation and hole-storage strategy is very promising for facilitating a lossless charge transfer during the PEC process.

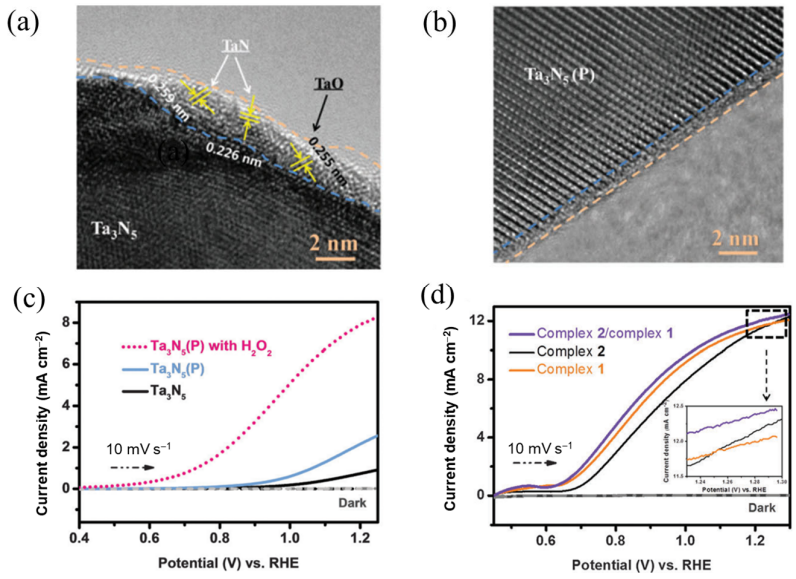


Figure 7. (**a**) The HRTEM image of the as-prepared Ta_3N_5 photoanode. (**b**) HRTEM image of the post-treated Ta_3N_5(P) photoanode. (**c**) Current–potential curves of pristine Ta_3N_5, Ta_3N_5(P) photoanodes and the Ta_3N_5(P) photoanode with H_2O_2 under AM 1.5 G simulated sunlight at 100 mW cm^{-2} in 1 M NaOH aqueous solution (pH = 13.6). (**d**) Current–potential curves of the complex 2/complex 1/$Ni(OH)_x$/Fh/TiO_x/Ta_3N_5(P) photoanode under AM 1.5 G simulated sunlight at 100 mW cm^{-2} in 1 M NaOH aqueous solution (pH = 13.6); the inset: the enlarged view of saturated photocurrent. Reproduced from [75] with permission.

4. Summary and Outlook

In summary, passivating the surface defects of photoelectrodes is very imperative for improved PEC performance. An effective passivation overlayer is generally required to

(1) be an ultrathin film less than 10 nm in thickness; (2) have a conformal coating to ensure sufficient passivation; (3) introduce no new defects; (4) be chemically inert. The passivation effect is generally represented by an onset potential shift (negative shift for photoanode and positive shift for photocathode), enhanced photocurrent density and occasionally improved PEC stability. The onset potential shift benefits from the elevated photovoltage, while the higher photocurrent profits from suppressed charge recombination. Boosted stability is generally ascribed to the physical isolation of an underlying light absorber by the chemically stable passivation overlayer.

Although surface passivation engineering itself could not enable overwhelming promotion in PEC activity, it would prominently reduce and even circumvent energy loss due to charge recombination at the surface defect sites, thus paving the way towards a highly efficient collection of charge carriers for interfacial chemical reactions. Therefore, surface passivation is considered pivotal in the design and fabrication of highly efficient photoelectrodes, which merits further and systematic investigation. Meanwhile, surface passivation is also significant in the fields of photocatalysis and photovoltaic cell, which share the same key point with photoelectrocatalysis in the survival of photogenerated charge carriers as many as possible.

Until now, various materials, including inorganic, organic and organic-inorganic hybrid passivation layers, have been developed by ALD, spin-coating, drop-coating, hydrothermal, solvent-thermal, electrochemical deposition, etc. Regardless, conformal overcoating can only be successfully prepared through either ALD or self-growth (self-assembling) technologies in view of their fundamental working principles, and the passivation effect could be evaluated with surface states capacitance from EIS, surface charge transfer rate constant and surface charge recombination rate constant from IMPS, induced photoluminescence intensity as well as carrier lifetime from TAS. However, the detailed mechanism for surface defect passivation remains unclear. Therefore, more effective preparation methods and passivation overlayers are expected to be further developed. Likewise, more credible and reliable characterization methods for surface states, as well as the passivation mechanisms, needed to be further explored.

Author Contributions: J.S.; writing—original draft preparation, review and editing, X.Z.; documental collection and discussion, C.L.; review, project administration. All authors have read and agreed to the published version of the manuscript.

Funding: This work was financially supported by the National Natural Science Foundation of China (nos. 22072152 and 22090034) and the National Key R&D Program of China (no. 2021YFB4000304). This work was also conducted by the National Natural Science Foundation of China and the Fundamental Research Center of Artificial Photosynthesis (no. 22088102).

Data Availability Statement: Not applicable.

Conflicts of Interest: The authors declare no conflict of interest.

References

1. Shi, J.Y.; Li, C. Photoelectrochemical Approach Using Photocatalysts. In *Solar to Chemical Conversion: Theory and Application*; Springer: Berlin/Heidelberg, Germany, 2016; pp. 319–344.
2. Jeong, H.K.; Hyo, E.K.; Jin, H.K.; Lee, J.S. Ferrites: Emerging Light Absorbers for Solar Water Splitting. *J. Mater. Chem. A* **2020**, *8*, 9447.
3. Hisatomi, T.; Kubota, J.; Domen, K. Recent Advances in Semiconductors for Photocatalytic and Photoelectrochemical Water Splitting. *Chem. Soc. Rev.* **2014**, *43*, 7520–7535. [CrossRef] [PubMed]
4. Fujishima, A.; Honda, K. Electrochemical Photolysis of Water at a Semiconductor Electrode. *Nature* **1972**, *238*, 37–38. [CrossRef]
5. Yu, Z.Y.; Duan, Y.; Feng, X.Y.; Yu, X.; Gao, M.R.; Yu, S.H. Clean and Affordable Hydrogen Fuel from Alkaline Water Splitting: Past, Recent Progress, and Future Prospects. *Adv. Mater.* **2021**, *33*, 2007100–2007134. [CrossRef] [PubMed]
6. Yao, T.T.; An, X.R.; Han, H.X.; Chen, Q.J.; Li, C. Photoelectrocatalytic Materials for Solar Water Splitting. *Adv. Energy Mater.* **2018**, *21*, 1800210. [CrossRef]
7. Jeongsuk, S.; Hiroshi, N.; Taro, Y.; Kazunari, D. Visible-Light-Responsive Photoanodes for Highly Active, Stable Water Oxidation. *Angew. Chem. Int. Ed.* **2018**, *57*, 8396–8415.

8. Lin, J.; Wang, W.L.; Li, G.Q. Modulating Surface/Interface Structure of Emerging InGaN Nanowires for Efficient Photoelectrochemical Water Splitting. *Adv. Funct. Mater.* **2020**, *30*, 2005677. [CrossRef]
9. Mohsin, A.M.; Muhammad, H.; Muhammad, W.A.; Zhang, H.B.; Muhammad, R.A.; Malik, A.; Muhammad, U.; Saad, W.; Habib, U.; Wang, C.D.; et al. Advanced Catalysts for Photoelectrochemical Water Splitting. *ACS Appl. Energy Mater.* **2021**, *4*, 12007–12031.
10. He, X.H.; Qiu, Y.C.; Yang, S.H. Fully-Inorganic Trihalide Perovskite Nanocrystals: A New Research Frontier of Optoelectronic Materials. *Adv. Mater.* **2017**, *29*, 1700775. [CrossRef]
11. Roger, I.; Shipman, M.A.; Symes, M.D. Earth-Abundant Catalysts for Electrochemical and Photoelectrochemical Water Splitting. *Nat. Rev. Chem.* **2017**, *1*, 0003. [CrossRef]
12. Hou, Y.; Zhuang, X.; Feng, X. Recent Advances in Earth-Abundant Heterogeneous Electrocatalysts for Photoelectrochemical Water Splitting. *Small Methods* **2017**, *1*, 1700090. [CrossRef]
13. Li, D.; Shi, J.Y.; Li, C. Transition-Metal-Based Electrocatalysts as Cocatalysts for Photoelectrochemical Water Splitting: A Mini Review. *Small* **2018**, *14*, 1704179. [CrossRef]
14. Zhang, D.D.; Shi, J.Y.; Zi, W.; Wang, P.P.; Liu, S.Z. Recent Advances in Photoelectrochemical Applications of Silicon Materials for Solar-to-Chemicals Conversion. *ChemSusChem* **2017**, *10*, 4324–4341. [CrossRef]
15. Ding, C.M.; Shi, J.Y.; Wang, Z.L.; Li, C. Photoelectrocatalytic Water Splitting: Significance of Cocatalysts, Electrolyte, and Interfaces. *ACS Catal.* **2017**, *7*, 675–688. [CrossRef]
16. Barroso, M.; Cowan, A.J.; Pendlebury, S.R.; Grätzel, M.; Klug, D.R.; Durrant, J.R. The Role of Cobalt Phosphate in Enhancing the Photocatalytic Activity of α-Fe_2O_3 toward Water Oxidation. *J. Am. Chem. Soc.* **2011**, *133*, 14868–14871. [CrossRef]
17. Jin, H.K.; Lee, J.S. Elaborately Modified $BiVO_4$ Photoanodes for Solar Water Splitting. *Adv. Mater.* **2019**, *31*, 1806938.
18. Liu, R.; Zheng, Z.; Joshua, S.; Yang, X.G. Enhanced Photoelectrochemical Water-Splitting Performance of Semiconductors by Surface Passivation Layers. *Energy Environ. Sci.* **2014**, *7*, 2504–2517. [CrossRef]
19. Zheng, J.Y.; Zhou, H.J.; Zou, Y.Q.; Wang, R.L.; Lyu, Y.H.; Jiang, S.P.; Wang, S.Y. Efficiency and Stability of Narrow-Gap Semiconductor-Based Photoelectrodes. *Energy Environ. Sci.* **2019**, *12*, 2345–2374. [CrossRef]
20. Zhou, D.H.; Fan, K. Recent Strategies to Enhance the Efficiency of Hematite Photoanodes in Photoelectrochemical Water Splitting. *Chin. J. Catal.* **2021**, *42*, 904–919. [CrossRef]
21. Vlachopoulos, N.; Gratzela, M.; Hagfeldt, A. Solid-State Dye-Sensitized Solar Cells Using Polymeric Hole Conductors. *RSC Adv.* **2021**, *11*, 39570–39581. [CrossRef]
22. Kobayashi, K.; Aikawa, Y.; Sukigara, M. Surface States at Semiconductor-Liquid Junction. *J. Appl. Phys.* **1983**, *5*, 54. [CrossRef]
23. Du, C.; Yang, X.G.; Mayer, M.T.; Hoyt, H.; Xie, J.; McMahon, G.; Bischoping, G.; Wang, D.W. Hematite-Based Water Splitting with Low Turn-On Voltages. *Angew. Chem. Int. Ed.* **2013**, *52*, 12692–12695. [CrossRef] [PubMed]
24. Retamal, J.R.D.; Chen, C.Y.; Lien, D.H.; Huang, M.R.S.; Lin, C.A.; Liu, C.P.; He, J.H. Concurrent Improvement in Photogain and Speed of a Metal Oxide Nanowire Photodetector through Enhancing Surface Band Bending via Incorporating a Nanoscale Heterojunction. *ACS Photonics* **2014**, *1*, 354–359. [CrossRef]
25. Varadhan, P.; Fu, H.C.; Priante, D.; Retamal, J.R.D.; Zhao, C.; Ebaid, M.; Ng, T.K.; Ajia, I.; Mitra, S.; Roqan, I.S.; et al. Surface Passivation of GaN Nanowires for Enhanced Photoelectrochemical Water-Splitting. *Nano Lett.* **2017**, *17*, 1520–1528. [CrossRef]
26. Formal, F.L.; Tetreault, N.; Cornuz, M.; Moehl, T.; Grätzel, M.; Sivula, K. Passivating Surface States on Water Splitting Hematite Photoanodes with Alumina Overlayers. *Chem. Sci.* **2011**, *2*, 737–743. [CrossRef]
27. Jang, J.W.; Du, C.; Ye, Y.F.; Lin, Y.J.; Yao, X.H.; Thorne, J.; Liu, E.; McMahon, G.; Zhu, J.F.; Javey, A.; et al. Enabling Unassisted Solar Water Splitting by Iron Oxide and Silicon. *Nat. Commun.* **2015**, *6*, 7447. [CrossRef]
28. Klahr, B.; Gimenez, S.; Francisco, F.S.; Hamann, T.; Bisquert, J. Water Oxidation at Hematite Photoelectrodes: The Role of Surface States. *J. Am. Chem. Soc.* **2012**, *134*, 4294–4302. [CrossRef]
29. Fathabadi, M.; Qorbani, M.; Sabbah, A.; Quadir, S.; Huang, C.; Chen, K.; Chen, L.; Naseri, N. An Ultrathin Amorphous Defective Co-doped Hematite Passivation Layer Derived Via An in Situ Electrochemical Method for Durable Photoelectrochemical Water Oxidation. *J. Mater. Chem. A* **2022**, *10*, 16655–16665. [CrossRef]
30. Li, T.F.; He, J.F.; Peña, B.; Berlinguette, C.P. Curing $BiVO_4$ Photoanodes with Ultraviolet Light Enhances Photoelectrocatalysis. *Angew. Chem. Int. Ed.* **2016**, *55*, 1769–1772. [CrossRef]
31. Trześniewski, B.J.; Digdaya, I.A.; Nagaki, T.; Ravishankar, S.; Cardona, I.; Vermaas, D.A.; Longo, A.; Gimenez, S.; Smith, W.A. Near-Complete Suppression of Surface Losses and Total Internal Quantum Efficiency in $BiVO_4$ Photoanodes. *Energy Environ. Sci.* **2017**, *10*, 1517–1529. [CrossRef]
32. Wang, L.; Gao, R.T. Stable Co-Catalyst-Free $BiVO_4$ Photoanodes with Passivated Surface States for Photocorrosion Inhibition. *Angew. Chem. Int. Ed.* **2020**, *59*, 23094–23099.
33. Hisatomi, T.; Formal, F.L.; Cornuz, M.; Brillet, J.; Tetreault, N.; Sivula, K.; Grätzel, M. Cathodic Shift in Onset Potential of Solar Oxygen Evolution on Hematite by 13-Group Oxide Overlayers. *Energy Environ. Sci.* **2011**, *4*, 2512–2515. [CrossRef]
34. Wan, X.K.; Xu, Y.B.; Wang, X.Y.; Guan, X.J.; Fu, Y.M.; Hu, C.; Hu, H.W.; Rong, N. Atomic Layer Deposition Assisted Surface Passivation on Bismuth Vanadate Photoanodes for Enhanced Solar Water Oxidation. *Appl. Surf. Sci.* **2022**, *573*, 151492. [CrossRef]
35. Dhandole, L.K.; Lee, H.H.; Chae, W.S.; Jang, J.S.; Lee, J.S. Self-Motivated, Thermally Oxidized Hematite Nanoflake Photoanodes: Effects of Pre-Polishing and ZrO_2 Passivation Layer. *J. Energy Chem.* **2022**, *65*, 415–423. [CrossRef]
36. Ren, S.J.; Sun, M.; Guo, X.T.; Liu, X.H.; Zhang, X.Y.; Wang, L. Interface-Confined Surface Engineering via Photoelectrochemical Etching toward Solar Neutral Water Splitting. *ACS Catal.* **2022**, *12*, 1686–1696. [CrossRef]

37. Guo, X.T.; Liu, X.H.; Wang, L. $NiMoO_x$ as A Highly Protective Layer Against Photocorrosion for Solar Seawater Splitting. *J. Mater. Chem. A* **2022**, *10*, 1270–1277. [CrossRef]
38. Yi, S.S.; Wang, Z.Y.; Li, H.M.; Zafar, Z.; Zhang, Z.T.; Zhang, L.Y.; Chen, D.L.; Liu, Z.Y.; Yue, X.Z. Coupling Effects of Indium Oxide Layer on Hematite Enabling Efficient Photoelectrochemical Water Splitting. *Appl. Catal. B Environ.* **2021**, *283*, 119649. [CrossRef]
39. Kim, W.; Tachikawa, T.; Monllor-Satoca, D.; Kim, H.; Majima, T.; Choi, W. Promoting Water Photooxidation on Transparent WO_3 Thin Films Using An Alumina Overlayer. *Energy Environ. Sci.* **2013**, *6*, 3732–3739. [CrossRef]
40. Zhao, Y.L.; Liu, G.J.; Wang, H.; Gao, Y.Y.; Yao, T.T.; Shi, W.W.; Li, C. Interface Engineering with An AlO_x Dielectric Layer Enabling an Ultrastable Ta_3N_5 Photoanode for Photoelectrochemical Water Oxidation. *J. Mater. Chem. A* **2021**, *9*, 11285–11290. [CrossRef]
41. Zhao, Y.L.; Xie, H.C.; Shi, W.W.; Wang, H.; Shao, C.Y.; Li, C. Unravelling the Essential Difference Between TiOx and AlOx Interface Layers on Ta_3N_5 Photoanode for Photoelectrochemical Water Oxidation. *J. Energy Chem.* **2022**, *64*, 33–37. [CrossRef]
42. Gui, Q.F.; Xu, Z.; Zhang, H.F.; Cheng, C.W.; Zhu, X.F.; Yin, M.; Song, Y.; Lu, L.F.; Chen, X.Y.; Li, D.D. Enhanced Photoelectrochemical Water Splitting Performance of Anodic TiO_2 Nanotube Arrays by Surface Passivation. *ACS Appl. Mater. Interfaces* **2014**, *6*, 17053–17058. [CrossRef] [PubMed]
43. Zhang, S.N.; Yu, T.T.; Liu, Y.; Feng, M.; Li, X.J.; Sun, W.X.; Wang, D.A. A New SiP QDs/TiO_2 NRs Composite Catalyst with Al_2O_3 Passivation Layer for Enhanced Photoelectrochemical Water Splitting. *Chem. Eng. J.* **2022**, *429*, 132248. [CrossRef]
44. Liu, C.; Zhang, C.; Yin, G.; Zhang, T.; Wang, W.; Ou, G.; Jin, H.; Chen, Z. A Three-Dimensional Branched TiO_2 Photoanode with an Ultrathin Al_2O_3 Passivation Layer and a NiOOH Cocatalyst toward Photoelectrochemical Water Oxidation. *ACS Appl. Mater. Interfaces* **2021**, *13*, 13301–13310. [CrossRef]
45. Liu, Y.P.; Xia, M.; Yao, L.; Mensi, M.; Ren, D.; Grätzel, M.; Sivula, K.; Guijarro, N. Spectroelectrochemical and Chemical Evidence of Surface Passivation at Zinc Ferrite ($ZnFe_2O_4$) Photoanodes for Solar Water Oxidation. *Adv. Funct. Mater.* **2021**, *31*, 2010081. [CrossRef]
46. Vanka, S.; Zhou, B.W.; Awni, R.A.; Song, Z.N.; Chowdhury, F.A.; Liu, X.D.; Hajibabaei, H.; Shi, W.; Xiao, Y.X.; Navid, I.A.; et al. InGaN/Si Double-Junction Photocathode for Unassisted Solar Water Splitting. *ACS Energy Lett.* **2020**, *5*, 3741–3751. [CrossRef]
47. Scheuermann, A.G.; Lawrence, J.P.; Ito, K.W.; Walsh, A.; Chidsey, C.E.D.; Hurley, P.K.; McIntyre, P.C. Design Principles for Maximizing Photovoltage in Metal-Oxide-Protected Water-Splitting Photoanodes. *Nat. Mater.* **2016**, *15*, 99–105. [CrossRef]
48. Zhang, D.D.; Cao, Y.X.; Karuturi, S.K.; Du, M.Y.; Liu, M.Y.; Xue, C.W.; Chen, R.T.; Wang, P.P.; Zhang, J.; Shi, J.Y.; et al. Enabling Unassisted Solar Water Splitting by Single-Junction Amorphous Silicon Photoelectrodes. *ACS Appl. Energy Mater.* **2020**, *3*, 4629–4637. [CrossRef]
49. Oh, K.; Mériadec, C.; Lassalle-Kaiser, B.; Dorcet, V.; Fabre, B.; Ababou-Girard, S.; Joanny, L.; Gouttefangeas, F.; Loget, G. Elucidating the Performance and Unexpected Stability of Partially Coated Water-Splitting Silicon Photoanodes. *Energy Environ. Sci.* **2018**, *11*, 2590–2599. [CrossRef]
50. Riyajuddin, S.; Sultana, J.; Siddiqui, S.A.; Kumar, S.; Badhwar, D.; Yadav, S.S.; Goyal, S.; Venkatesan, A.; Chakraverty, S.; Ghosh, K. Silicon Nanowire–Ta_2O_5–NGQD Heterostructure: An Efficient Photocathode for Photoelectrochemical Hydrogen Evolution. *Sustain. Energy Fuels* **2022**, *6*, 197–208. [CrossRef]
51. Liu, B.; Feng, S.J.; Yang, L.F.; Li, C.C.; Luo, Z.B.; Wang, T.; Gong, J.L. Bifacial Passivation of n-Silicon Metal–Insulator–Semiconductor Photoelectrodes for Efficient Oxygen and Hydrogen Evolution Reactions. *Energy Environ. Sci.* **2020**, *13*, 221–228. [CrossRef]
52. Choi, S.; Hwang, J.; Lee, T.H.; Kim, H.; Hong, S.; Kim, C.; Choi, M.; Park, H.K.; Bhat, S.; Suh, J.M.; et al. Photoelectrochemical Hydrogen Production at Neutral pH Phosphate Buffer Solution Using TiO_2 Passivated InAs Nanowire/p-Si Heterostructure Photocathode. *Chem. Eng. J.* **2020**, *392*, 123688. [CrossRef]
53. Chen, C.; Chen, P.; Basu, M.; Yang, K.; Lu, Y.R.; Dong, C.L.; Ma, C.G.; Shen, C.C.; Hu, S.F.; Liu, R.S. An Integrated Cobalt Disulfide (CoS_2) Co-Catalyst Passivation Layer On Silicon Microwires for Photoelectrochemical Hydrogen Evolution. *J. Mater. Chem. A* **2015**, *3*, 23466–23476. [CrossRef]
54. Bao, X.Q.; Petrovykh, D.Y.; Alpuim, P.; Stroppa, D.G.; Guldris, N.; Fonseca, H.; Costa, M.; Gaspar, J.; Jin, C.; Liu, L.F. Amorphous Oxygen-Rich Molybdenum Oxysulfide Decorated p-Type Silicon Microwire Arrays for Efficient Photoelectrochemical Water Reduction. *Nano Energy.* **2015**, *16*, 130–142. [CrossRef]
55. Liu, G.J.; Eichhorn, J.; Jiang, C.M.; Scott, M.; Hess, L.; Gregoire, J.; Haber, J.; Sharp, I.; Toma, F. Interface Engineering for Light-Driven Water Oxidation: Unravelling the Passivating and Catalytic Mechanism in $BiVO_4$ Overlayers. *Sustain. Energy Fuels* **2019**, *3*, 127–135. [CrossRef]
56. Thorne, J.E.; Jang, J.W.; Liu, E.Y.; Wang, D. Understanding the Origin of Photoelectrode Performance Enhancement by Probing Surface Kinetics. *Chem. Sci.* **2016**, *7*, 3347–3354. [CrossRef]
57. Da, P.; Cha, M.Y.; Sun, L.; Wu, Y.Z.; Wang, Z.S.; Zheng, G.F. High-Performance Perovskite Photoanode Enabled by Ni Passivation and Catalysis. *Nano Lett.* **2015**, *15*, 3452–3457. [CrossRef]
58. Kenney, M.; Gong, M.; Li, Y.G.; Wu, J.; Feng, J.; Lanza, M.; Dai, H.J. High-Performance Silicon Photoanodes Passivated with Ultrathin Nickel Films for Water Oxidation. *Science* **2013**, *342*, 837–839. [CrossRef]
59. Yu, X.W.; Yang, P.; Chen, S.; Zhang, M.; Shi, G.Q. NiFe Alloy Protected Silicon Photoanode for Efficient Water Splitting. *Adv. Energy Mater.* **2017**, *7*, 1601805. [CrossRef]

60. Jia, M.Y.; Xiong, W.P.; Yang, Z.H.; Cao, J.; Zhang, Y.R.; Xiang, Y.P.; Xu, H.Y.; Song, P.P.; Xu, Z.Y. Metal-Organic Frameworks and Their Derivatives-Modified Photoelectrodes for Photoelectrochemical Applications. *Coord. Chem. Rev.* **2021**, *434*, 213780. [CrossRef]
61. Yoon, J.W.; Kim, J.H.; Kim, C.; Jang, H.W.; Lee, J.H. MOF-Based Hybrids for Solar Fuel Production. *Adv. Energy Mater.* **2021**, *11*, 2003052. [CrossRef]
62. Li, X.; Liu, S.W.; Fan, K.; Liu, Z.Q.; Song, B.; Yu, J.G. MOF-Based Transparent Passivation Layer Modified ZnO Nanorod Arrays for Enhanced Photo-Electrochemical Water Splitting. *Adv. Energy Mater.* **2018**, *8*, 1800101. [CrossRef]
63. Yu, H.H.; Tan, X.R.; Zhang, L.; Yang, H.M.; Zhu, P.H.; Yan, Z.; Gao, C.M.; Yu, J.H. Metal-Organic Framework-Enabled Surface State Passivation Integrating with Single-Nuclease-Propelled Multistage Amplification for Ultrasensitive Lab-on-Paper Photoelectrochemical Biosensing. *Chem. Eng. J.* **2022**, *450*, 137955. [CrossRef]
64. Dong, Y.J.; Liao, J.F.; Kong, Z.C.; Xu, Y.F.; Chen, Z.J.; Chen, H.Y.; Kuang, D.B.; Fenske, D.; Su, C.Y. Conformal Coating of Ultrathin Metal-Organic Framework on Semiconductor Electrode for Boosted Photoelectrochemical Water Oxidation. *Appl. Catal. B Environ.* **2018**, *237*, 9–17. [CrossRef]
65. Wu, F.K.; Xie, J.L.; You, Y.; Zhao, Z.Y.; Wang, L.L.; Chen, X.Y.; Yang, P.P.; Huang, Y.L. Cobalt Metal-Organic Framework Ultrathin Cocatalyst Overlayer for Improved Photoelectrochemical Activity of Ti-Doped Hematite. *ACS Appl. Energy Mater.* **2020**, *3*, 4867–4876. [CrossRef]
66. Wang, Z.Y.; Li, H.M.; Yi, S.S.; You, M.Z.; Jing, H.J.; Yue, X.Z.; Zhang, Z.T.; Chen, D.L. In-Situ Coating of Multifunctional FeCo-Bimetal Organic Framework Nanolayers on Hematite Photoanode for Superior Oxygen Evolution. *Appl. Catal. B Environ.* **2021**, *297*, 120406. [CrossRef]
67. Sun, M.H.; Joyce, H.J.; Gao, Q.; Tan, H.H.; Jagadish, C.; Ning, C.Z. Removal of Surface States and Recovery of Band-Edge Emission in InAs Nanowires through Surface Passivation. *Nano Lett.* **2012**, *12*, 3378–3384. [CrossRef]
68. Tajik, N.; Haapamaki, C.M.; LaPierre, R.R. Photoluminescence Model of Sulfur Passivated p-InP Nanowires. *Nanotechnology* **2012**, *23*, 315703. [CrossRef]
69. Cui, W.; Wu, S.; Chen, F.J.; Xia, Z.H.; Li, Y.G.; Zhang, X.H.; Song, T.; Lee, S.; Sun, B.Q. Silicon/Organic Heterojunction for Photoelectrochemical Energy Conversion Photoanode with a Record Photovoltage. *ACS Nano* **2016**, *10*, 9411–9419. [CrossRef]
70. Lin, J.; Yu, Y.; Zhang, Z.; Gao, F.; Liu, S.; Wang, W.; Li, G. A Novel Approach for Achieving High-Efficiency Photoelectrochemical Water Oxidation in InGaN Nanorods Grown on Si System: MXene Nanosheets as Multifunctional Interfacial Modifier. *Adv. Funct. Mater.* **2020**, *30*, 1910479. [CrossRef]
71. Kim, J.H.; Choi, Y.; Kim, J.H.; Kim, J.; Kim, Y.K.; Kim, J.K.; Lee, J.S. $ZnFe_2O_4$ Dendrite/SnO_2 Helix 3D Hetero-Structure Photoanodes for Enhanced Photoelectrochemical Water Splitting: Triple Functions of SnO_2 Nanohelix. *Small* **2021**, *17*, 2103861. [CrossRef]
72. Ahn, H.; Yoon, K.; Kwak, M.; Jang, J. A Titanium-Doped SiOx Passivation Layer for Greatly Enhanced Performance of a Hematite-Based Photoelectrochemical System. *Angew. Chem. Int. Ed.* **2016**, *55*, 9922–9926. [CrossRef]
73. Liu, G.J.; Shi, J.Y.; Zhang, F.X.; Chen, Z.; Han, J.F.; Ding, C.M.; Chen, S.S.; Wang, Z.L.; Han, H.X.; Li, C. A Tantalum Nitride Photoanode Modified with a Hole-Storage Layer for Highly Stable Solar Water Splitting. *Angew. Chem. Int. Ed.* **2014**, *53*, 7295–7299. [CrossRef]
74. Liu, G.J.; Fu, P.; Zhou, L.Y.; Yan, P.L.; Ding, C.M.; Shi, J.Y.; Li, C. Efficient Hole Extraction from Hole-Storage-Layer-Stabilized Tantalum Nitride Photoanode for Solar Water Splitting. *Chem. Eur. J.* **2015**, *21*, 9624–9628. [CrossRef]
75. Liu, G.J.; Ye, S.; Yan, P.; Xiong, F.Q.; Fu, P.; Wang, Z.L.; Chen, Z.; Shi, J.Y.; Li, C. Enabling an Integrated Tantalum Nitride Photoanode to Approach the Theoretical Photocurrent Limit for Solar Water Splitting. *Energy Environ. Sci.* **2016**, *9*, 1327–1334. [CrossRef]
76. Wang, P.P.; Li, D.; Chi, H.B.; Zhao, Y.L.; Wang, J.H.; Li, D.F.; Pang, S.; Fu, P.; Shi, J.Y.; Li, C. Unveiling the Hydration Structure of Ferrihydrite for Hole Storage in Photoelectrochemical Water Oxidation. *Angew. Chem. Int. Ed.* **2021**, *60*, 6691–6698. [CrossRef]
77. Wang, P.P.; Fu, P.; Ma, J.P.; Gao, Y.Y.; Li, Z.; Wang, H.; Fan, F.T.; Shi, J.Y.; Li, C. Ultrathin Cobalt Oxide Interlayer Facilitated Hole Storage for Sustained Water Oxidation Over Composited Tantalum Nitride Photoanodes. *ACS Catal.* **2021**, *11*, 12736–12744. [CrossRef]
78. Wang, P.P.; Ding, C.M.; Li, D.F.; Cao, Y.M.; Li, Z.; Wang, X.L.; Shi, J.Y.; Li, C. Coupling Effect Between Hole Storage and Interfacial Charge Transfer over Ultrathin CoPi Modified Hematite Photoanode. *Dalton Trans.* **2022**, *51*, 9247–9255. [CrossRef]
79. Xiao, Y.; Feng, C.; Fu, J.; Wang, F.; Li, C.; Kunzelmann, V.F.; Jiang, C.M.; Nakabayashi, M.; Shibata, N.; Sharp, I.D.; et al. Band Structure Engineering and Defect Control of Ta_3N_5 for Efficient Photoelectrochemical Water Oxidation. *Nat. Catal.* **2020**, *3*, 932–940. [CrossRef]
80. Zhang, D.D.; Du, M.Y.; Wang, P.P.; Wang, H.; Shi, W.W.; Gao, Y.Y.; Karuturi, S.; Catchpole, K.; Zhang, J.; Fan, F.T.; et al. Hole-Storage Enhanced a-Si Photocathodes for Efficient Hydrogen Production. *Angew. Chem. Int. Ed.* **2021**, *60*, 11966–11972. [CrossRef]

Disclaimer/Publisher's Note: The statements, opinions and data contained in all publications are solely those of the individual author(s) and contributor(s) and not of MDPI and/or the editor(s). MDPI and/or the editor(s) disclaim responsibility for any injury to people or property resulting from any ideas, methods, instructions or products referred to in the content.